Development 140, 2755-2764 (2013) doi:10.1242/dev.092825

miR-34b regulates multiciliogenesis during organ formation in zebrafish

Lei Wang[1,*], Cong Fu[1,*], Hongbo Fan[1], Tingting Du[1], Mei Dong[1], Yi Chen[1], Yi Jin[1], Yi Zhou[2], Min Deng[1], Aihua Gu[3,‡], Qing Jing[1,‡], Tingxi Liu[1,§] and Yong Zhou[1,‡]

SUMMARY

Multiciliated cells (MCCs) possess multiple motile cilia and are distributed throughout the vertebrate body, performing important physiological functions by regulating fluid movement in the intercellular space. Neither their function during organ development nor the molecular mechanisms underlying multiciliogenesis are well understood. Although dysregulation of members of the miR-34 family plays a key role in the progression of various cancers, the physiological function of miR-34b, especially in regulating organ formation, is largely unknown. Here, we demonstrate that miR-34b expression is enriched in kidney MCCs and the olfactory placode in zebrafish. Inhibiting miR-34b function using morpholino antisense oligonucleotides disrupted kidney proximal tubule convolution and the proper distribution of distal transporting cells and MCCs. Microarray analysis of gene expression, cilia immunostaining and a fluid flow assay revealed that miR-34b is functionally required for the multiciliogenesis of MCCs in the kidney and olfactory placode. We hypothesize that miR-34b regulates kidney morphogenesis by controlling the movement and distribution of kidney MCCs and fluid flow. We found that *cmyb* was genetically downstream of *miR-34b* and acted as a key regulator of multiciliogenesis. Elevated expression of *cmyb* blocked membrane docking of centrioles, whereas loss of *cmyb* impaired centriole multiplication, both of which resulted in defects in the formation of ciliary bundles. Thus, miR-34b serves as a guardian to maintain the proper level of *cmyb* expression. In summary, our studies have uncovered an essential role for miR-34b-Cmyb signaling during multiciliogenesis and kidney morphogenesis.

KEY WORDS: Cell migration, Kidney, microRNA, Multiciliogenesis, Olfactory placode, *mir34b*

INTRODUCTION

Fluid flow and the resulting shear forces are important for specific aspects of organogenesis and tissue development, such as the establishment of left-right asymmetry, the formation of heart chambers, angiogenesis, hematopoietic stem cell emergence and neural progenitor cell migration (Freund et al., 2012; Lehtinen et al., 2011; Poelmann et al., 2008). In a dynamic fluid environment driven by cilia, the proper distribution of cilia along channel and cavity ducts, together with coordinated ciliary beating, control the force and direction of fluid flow. However, the principles that define cilia distribution and the resulting physiological implications remain unclear. Multiciliated cells (MCCs) feature multiple motile cilia on the cell surface and are widely distributed throughout the vertebrate body to regulate fluid movement in the intercellular space (Fliegauf et al., 2007; Hildebrandt et al., 2011). These cells remove mucus from the surface of the respiratory system, drive cerebrospinal fluid in the brain, perform olfactory functions and move ova in the oviducts. A recent report showed that Notch signaling is essential for the progression of multiciliogenesis (Marcet et al., 2011). However, research on the cellular and molecular mechanisms of multiciliogenesis is still in the early stages.

During zebrafish development, MCCs are abundantly distributed throughout the pronephric ducts and olfactory placode; thus, these structures serve as good models with which to study multiciliogenesis and its function in organ formation. A crucial process during organ formation is cellular rearrangement via coordinated cell migration, as is observed in the developing heart, liver, mammary gland and kidney (Abu-Issa and Kirby, 2007; Dressler, 2006; Ewald et al., 2008; Si-Tayeb et al., 2010). The vertebrate kidney is essential for blood homeostasis and the clearance of body waste. It is formed via the differentiation of multiple cell types and subsequent morphogenic cell movements (Dressler, 2006). Abnormalities in kidney and urinary tract development can lead to childhood kidney diseases, such as aplasia/dysplasia, vesicoureteral reflux and renal tubular dysgenesis.

The zebrafish has become an excellent model organism for kidney research due to the conservation of cellular and molecular regulatory pathways among vertebrates and the structural simplicity of the embryonic kidney (Drummond, 2005; Ebarasi et al., 2011). In zebrafish, morphogenic cell movement within the kidney begins at 24 hours post-fertilization (hpf), as a means of collective cell migration. The distal tubule cells then migrate proximally and manifest the position of each nephron segment. Subsequently, the proximal cells become convoluted by 72 hpf. Fluid flow, which is driven by blood pressure and cilia beating, is required for this process. The zebrafish pronephric ducts are filled with scattered single cilia prior to 30 hpf. Thereafter, organized cilia bundles replace the single cilia on the surface of cells in the middle pronephric ducts, whereas the single cilia at the proximal and distal ducts are preserved. The cilia in the middle pronephric ducts beat in a synchronized manner to drive the fluid flow from the anterior to

[1]Key Laboratory of Stem Cell Biology and State Key Laboratory of Medical Genomics and Laboratory of Development and Diseases, Institute of Health Sciences, Shanghai Institutes for Biological Sciences, Chinese Academy of Sciences and Shanghai Jiao Tong University School of Medicine, and Shanghai Institute of Hematology, RuiJin Hospital, Shanghai Jiao Tong University School of Medicine, Shanghai 200025, People's Republic of China. [2]Boston Children's Hospital, Harvard Medical School, Boston, MA 02115, USA. [3]School of Public Health, Nanjing Medical University, Nanjing 210029, People's Republic of China.

*These authors contributed equally to this work
‡Authors for correspondence (aihuagu@njmu.edu.cn; qjing@sibs.ac.cn; zhouyong@sibs.ac.cn)
§Deceased

Accepted 24 April 2013

posterior region of the duct (Kramer-Zucker et al., 2005; Liu et al., 2007; Ma and Jiang, 2007; Sullivan-Brown et al., 2008).

Although the relationship between ciliary defects and cystic kidney disease has been well established, little is known about the function of the cilia bundles in kidney development or about the molecular mechanisms that control multiciliogenesis. Disruption of fluid flow by a mechanical or genetic method can block both the migration of tubule cells and proximal tubule convolution (Vasilyev et al., 2009). However, the molecular mechanisms that regulate these processes are poorly understood.

A variety of microRNA species modulate organogenesis in vertebrates; however, few have been shown to participate in kidney morphogenesis and olfactory organ development. The miR-34 family, which is highly conserved in vertebrates, is downregulated in many cancer types and plays an important role in carcinogenesis. By functioning downstream of p53 signaling, miR-34 family members regulate cell proliferation, migration and apoptosis (Dressler, 2006; He et al., 2007; Hermeking, 2010). Under normal physiological conditions, miR-34a is involved in neuronal development and miR-34c is functionally required for spermatogenesis (Agostini et al., 2011a; Agostini et al., 2011b; Bouhallier et al., 2010; Liu et al., 2012). However, the role of miR-34b in development is largely unknown. Here, we report that the expression of miR-34b is enriched in both kidney MCCs and the olfactory placode and that miR-34b is required for normal kidney morphogenesis and olfactory organ development. miR-34b regulates multiciliogenesis, which is essential for the proper migration of kidney cells. In addition, we demonstrate that *cmyb* is a key mediator of this process.

MATERIALS AND METHODS

Ethics statement

The zebrafish facility and zebrafish study were approved by the Institutional Review Board of the Institute of Health Sciences, Shanghai Institutes of Biological Sciences, Chinese Academy of Sciences (Shanghai, China).

Zebrafish lines

Wild-type *AB* and transgenic *Tg(cmyb:EGFP)* (North et al., 2007), *cmyb*^{hkz} and *Tg(hsp70:cmyb)* (Zhang et al., 2011) zebrafish were raised under standard conditions. *Tg(hsp70:cmyb)* embryos and siblings were heat shocked at 40°C for 1 hour every 3 hours from 18 hpf and fixed at 36, 48 or 72 hpf for analysis and identified by genomic PCR.

Microinjection

Morpholinos (Gene Tools) and miR-34b duplex (GenePharma, Shanghai) were injected in 1- to 2-cell stage embryos. Morpholinos and duplexes (including dosages) are detailed in supplementary material Table S1.

Embryo staining

The miR-34b *in situ* hybridization was performed at 50°C using miRCURY detection probe according to the manufacturer's protocol (Exiqon). For the *in situ* hybridization and immunofluorescence double staining, fluorescent *in situ* hybridization was performed first according to published protocols (Brend and Holley, 2009) using a Cy3 kit (Perkin Elmer); then, the antibody staining was performed using rabbit anti-GFP polyclonal serum (1:500; Invitrogen) and goat anti-rabbit Alexa Fluor 488 antibody (1:500; Invitrogen). For immunofluorescence double staining, first primary antibody against GFP was mixed with antibody against acetylated tubulin 6-11b-1, γ-tubulin (1:500; Sigma-Aldrich) or against PH3 (1:500; Santa Cruz), followed by staining with the secondary antibody (1:500; Alexa Fluor 488 or 546) the next day. TUNEL staining was performed as described (Fu et al., 2009).

Cell sorting, microarray and quantitative PCR analysis

A tissue block containing the kidney was dissected from *Tg(cmyb:EGFP)* embryos 3 days post-fertilization (dpf) (supplementary material Fig. S3A), digested with 0.25% trypsin (Invitrogen) for 1 hour and filtered through a 40 μm cell strainer (BD Falcon). About 20,000 GFP$^+$ cells were sorted out using a FACSAria flow cytometer (BD) and used for RNA extraction. The percentage of GFP$^+$ cells in the tissue block was 0.4±0.05%. Greater than 90% of cells were viable before and after cell sorting as counted by Trypan Blue staining.

For microarray analysis (performed by the Shanghai Biochip Company), ~100 ng total RNA was used for cDNA generation, amplified and hybridized to Affymetrix Zebrafish Genome Arrays. Two independent sets of biological replicates (miR-34b MO and Ctrl MO) were used. The data were normalized using MAS 5.0 (Affymetrix). Student's *t*-test was performed to identify genes with a significant change in expression (P<0.05). Genes with greater than 1.5-fold change in expression were used for gene ontology (GO) analysis by DAVID (Huang et al., 2009). The GOTERM_BP_FAT category was used and GO terms with P<0.05 were listed according to the fold enrichment score. The microarray data have been deposited in the Array Express database (www.ebi.ac.uk/arrayexpress) under accession number E-MEXP-3893.

Quantitative RT-PCR (QRT-PCR) reactions were performed using the Roche 480 system. Each sample was tested in triplicate and β-*actin 1* was used to normalize signals for each queried transcript using the ΔΔCt method. Primers are listed in supplementary material Table S2.

Cell tracking

Tg(cmyb:EGFP) embryos at 51-72 hpf were mounted in a self-made imaging chamber as previously reported (Kamei and Weinstein, 2005). Time-lapse imaging was performed using a Leica TCS SP5 confocal microscope with 10× objective every 10 minutes. Cell migration analysis was performed using Image-Pro Analyzer 7.0 (Media Cybernetics) image analysis software according to a published protocol (Hall et al., 2009); each embryo was captured independently and combined using Corel Videostudio Pro X2. Cells that were successfully tracked at all the time points were selected and their migration distances used for statistical analysis. Three independent experiments were performed for miR-34b MO- or Ctrl MO-injected *Tg(cmyb:EGFP)* embryos.

Urine dye excretion assay

A 5% solution of tetramethylrhodamine-conjugated 70 kDa dextran (Molecular Probes) was injected into the common cardinal vein of 3.5-dpf embryos (Drummond and Davidson, 2010; Malicki et al., 2011) and urine excretion at the cloaca was recorded using a SteREO Discovery V20 fluorescence stereomicroscope (Carl Zeiss). The time from injection to the first visible urine excretion at the cloaca was used for statistical analysis.

MicroRNA target prediction and reporter assay

The miR-34b target site (MRE) was predicted by MicroCosm (EBI, EMBL) and KeyTar (L. H. Lai group, East China Normal University) (supplementary material Table S3). 2×MRE or 3′ UTR was cloned and fused to *EGFP* in the pCS2$^+$ plasmid (Fu et al., 2009). Capped mRNAs (with *DsRed* as an internal control) were synthesized with the mMESSAGE mMACHINE kit (Ambion) and injected with miR-34b duplex or Ctrl duplex as described previously (Fu et al., 2009).

Statistical analysis

All statistics were performed using an unpaired Student's *t*-test.

RESULTS

miR-34b expression is enriched in MCCs in the kidney and the olfactory placode

A large-scale microRNA expression study previously showed that miR-34b is expressed in a punctate pattern along the zebrafish pronephric ducts at 3 and 5 dpf (Wienholds et al., 2005). We further characterized the expression of miR-34b during early development by whole-mount *in situ* hybridization (WISH). There was no maternal miR-34b expression; enriched zygotic expression along the pronephric ducts was detected beginning at 24 hpf and expression in the olfactory placode was detectable from 36 hpf (Fig. 1E, arrows;

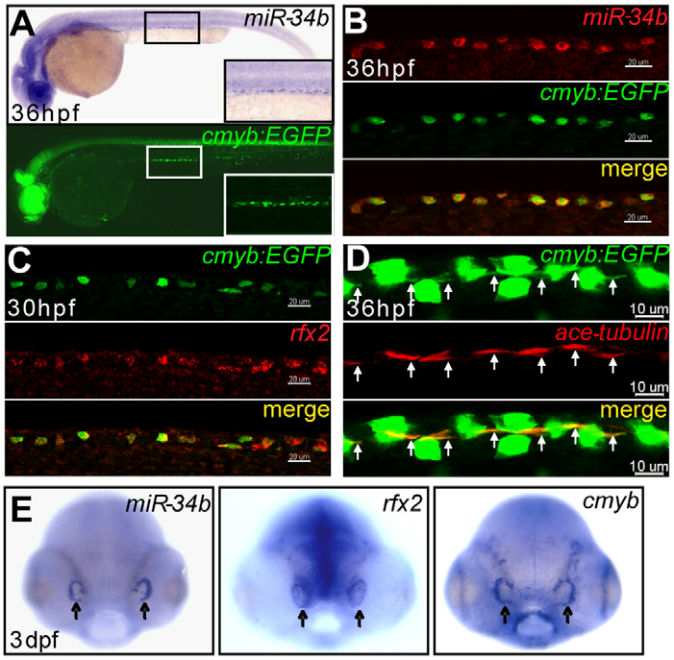

Fig. 1. miR-34b expression is enriched in kidney MCCs and in the olfactory placode. (**A**) Lateral view of a 36-hpf zebrafish embryo after *in situ* hybridization shows that the expression of miR-34b resembles the pattern of kidney cells labeled by *Tg(cmyb:EGFP)*. A magnified lateral view (inset) shows the labeled cells distributed in a punctate pattern. (**B**,**C**) Confocal images (lateral view) of the kidney region show the colocalization of miR-34b, *rfx2* (red, WISH) and Cmyb:EGFP (green, immunostaining). (**D**) Confocal images of the kidney region show that each Cmyb:EGFP$^+$ cell (green, immunostaining; overexposed to show the cilia bundle region, arrows) has a cilia bundle (immunolabeled using anti-acetylated tubulin antibody, red, arrows). The GFP staining is weaker in B and C than in D owing to the different staining methods. (**E**) Dorsal view of a 3-dpf embryo after *in situ* hybridization shows expression of miR-34b, *rfx2* and *cmyb* in the olfactory placode (arrows). Scale bars: 20 μm in B,C; 10 μm in D.

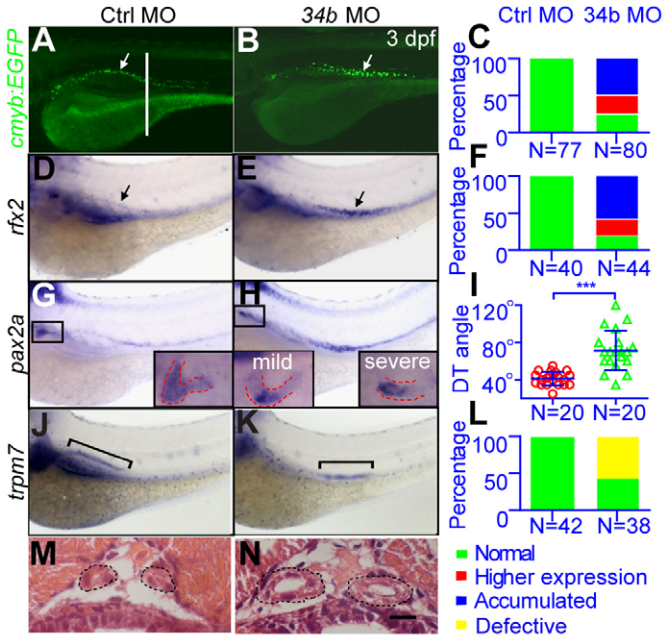

Fig. 2. Loss of miR-34b disrupts kidney morphogenesis. (**A-F**) *In situ* hybridization with the *rfx2* probe and images of the *Tg(cmyb:EGFP)* embryo show that MCCs accumulate in the middle part of the pronephric duct (arrows) in miR-34b morphants at 3 dpf. C and F show the percentage of embryos with abnormal *cmyb*$^+$ (shown in A,B) or *rfx2*$^+$ (shown in D,E) MCCs. Embryos with accumulated MCCs (Accumulated) or higher expression levels of *cmyb* or *rfx2* (Higher expression) were counted. (**G-I**) A magnified lateral view (with a small angle to dorsal) of a 3-dpf embryo after *in situ* hybridization with the *pax2* probe shows that proximal tubule convolution is blocked at 3 dpf in miR-34b morphants. Examples of normal proximal tubule convolution (G) and of mild and severe defects (H) are illustrated in the insets. The angle between the kidney duct and tubule (DT angle) was measured. Each circle/triangle in I represents an embryo. Mean ± s.d. ***P<0.0001 (unpaired t-test). (**J-L**) Lateral view of a 3-dpf embryo after *in situ* hybridization with the *trpm7* probe shows that transporting epithelial cells accumulate in the middle region (bracket) of the pronephric duct 3 dpf after miR-34b knockdown. L shows the percentage of embryos with abnormal distribution of *trpm7*$^+$ transporting epithelial cells (Defective). (**M**,**N**) Hematoxylin and Eosin (H&E) staining on a transverse section (plane indicated by the white line in A) shows the enlarged tubule diameter (outlined) after miR-34b knockdown.

supplementary material Fig. S1). This expression pattern resembled the pattern of *cmyb*-EGFP-labeled kidney cells along the pronephric ducts in *Tg(cmyb:EGFP)* embryos (Bertrand et al., 2008; North et al., 2007) (Fig. 1A). These cells were thought to be MCCs and to possess hematopoietic potential (Bertrand et al., 2008; Vasilyev et al., 2009). Double fluorescent staining using an anti-EGFP antibody and a miR-34b probe showed that miR-34b is co-expressed with the *cmyb*-EGFP transgene (Fig. 1B). Surprisingly, we observed a ring-like pattern of miR-34b expression, consistent with its location in the cytoplasm, indicating that miR-34b functions mainly in the cytoplasm.

To further clarify whether the kidney cells labeled in the *Tg(cmyb:EGFP)* embryos are MCCs, we performed double fluorescent staining using anti-EGFP antibodies and RNA probes for *rfx2*, a known molecular marker of MCCs (Liu et al., 2007; Ma and Jiang, 2007). As shown in Fig. 1C, EGFP$^+$ cells in the pronephric duct colocalized with *rfx2*. These results confirmed that *cmyb*-EGFP$^+$ cells in the *Tg(cmyb:EGFP)* embryos are multiciliated kidney cells. Immunostaining with anti-EGFP and anti-acetylated tubulin antibodies showed that each EGFP$^+$ cell had a cilia bundle consisting of multiple cilia (Fig. 1D). We also found expression of miR-34b, *rfx2* and *cmyb* in the olfactory placode (Fig. 1E), where multiciliated sensory neurons reside. These results demonstrate that miR-34b expression is enriched in *rfx2*$^+$ and *cmyb*$^+$ MCCs in the kidney and olfactory placode. In the following experiments, we focused our efforts on the kidney to study the function of miR-34b in MCCs.

miR-34b is required for kidney morphogenesis and *cmyb*$^+$ MCCs are not hematopoietic cells

To study the *in vivo* function of miR-34b, two morpholinos (MOs) (miR-34b MO1 and MO2) were designed to block the maturation of miR-34b (supplementary material Fig. S2A). These MOs inhibited the maturation of miR-34b without causing circulation defects or global developmental abnormalities in the morphants, such as developmental retardation or body symmetry defects. These observations were consistent with the restricted expression pattern of miR-34b. However, kidney morphogenesis was clearly disrupted in these embryos at 3 dpf (Fig. 2). Both MOs led to similar kidney defects (supplementary material Fig. S2B), although miR-34b MO1

gave stronger and more consistent phenotypes and was therefore used in subsequent experiments.

In the miR-34b morphants, there was a strong accumulation of *rfx2*$^+$ *cmyb*$^+$ MCCs in the middle region of the pronephric ducts (Fig. 2A-F). Using the pronephric epithelial marker *pax2*, we found that proximal tubule convolution was blocked (Fig. 2G-I). The distribution of the distal *trpm7*$^+$ transporting epithelial cells was also abnormal; these cells were shorter than normal and failed to extend towards the head kidney (Fig. 2J-L). The tubule diameter was severely expanded compared with that of control animals [41±8 μm (*n*=12) versus 25±5 μm (*n*=10), mean ± s.d.; *P*<0.0001, Fig. 2M,N].

The *cmyb*-EGFP$^+$ cells along the pronephric duct have hematopoietic potential (Bertrand et al., 2008). We analyzed the development of different blood lineages in the miR-34b morphants by WISH at 30 and 36 hpf and at 2, 3 and 5 dpf using *scl* (*tal1* – Zebrafish Information Network) to monitor progenitor cells, *mpo* (*mpx*) to mark the myeloid lineage, *gata1* and hemoglobin α embryonic 1 (*hbae1*) to label the erythroid lineage, *CD41* (*itga2b*) to mark thrombocytes and *rag1* to indicate T-cell development. There were no differences in overall cell numbers or cell lineage types detected at any of the hematopoietic sites investigated, including the head kidney (supplementary material Fig. S2D). We conclude that the miR-34b-expressing cells in the pronephric duct region were not hematopoietic stem cells prior to 5 dpf.

The abnormal distribution of MCCs is caused by abnormal cell migration

To understand the cellular basis of the observed kidney phenotypes, we first focused on the MCCs, in which miR-34b is highly expressed. MCCs may accumulate in the middle region of the pronephric ducts at 3 dpf for a number of reasons. It could be attributed to overproliferation or decreased apoptosis of MCCs in this region. Alternatively, there may be biased differentiation of bipotential precursor cells toward an MCC fate at the expense of *trpm7*$^+$ transporting epithelial cells (Liu et al., 2007; Ma and Jiang, 2007). It is also possible that cell migration is blocked in these embryos. To discriminate between these possibilities, we first manually counted the number of MCCs and found that this value was normal from 36 to 48 hpf in the miR-34b morphants (supplementary material Fig. S2C). Next, we analyzed cell proliferation and apoptosis by phosphohistone H3 (PH3) and TUNEL staining, respectively, at 36, 48 and 72 hpf. In both the controls and miR-34b morphants, only a few MCCs were PH3$^+$, and no increase in PH3 staining was found in the MCCs at any of the developmental stages analyzed (Fig. 3A). There was also no change in TUNEL staining of the pronephric duct region in the miR-34b morphants (Fig. 3B). These results demonstrated that the accumulation of MCCs that is observed when the levels of miR-34b are reduced is not due to alterations in either cell proliferation or apoptosis. We then analyzed the balance of bipotential cell differentiation by *trpm7* WISH at 36 hpf. In the miR-34b morphants, both the distribution of *trpm7*$^+$ cells and the number of MCCs were normal in comparison to the control animals (Fig. 3C,D; supplementary material Fig. S2C), suggesting that there is no biased differentiation of precursor cells toward MCCs at the expense of *trpm7*$^+$ transporting epithelial cells.

Finally, we tracked the migration of the MCCs by confocal time-lapse imaging from 51 to 72 hpf using *Tg(cmyb:EGFP)* fish. We found that the migration distance of the MCCs in miR-34b morphants was significantly decreased compared with that of control animals [66±11 μm (*n*=10) versus 110±23 μm (*n*=10); Fig. 3E-G]. The migration of the cells in the proximal ducts was substantially blocked, whereas migration in the distal ducts was almost normal (Fig. 3E,F; supplementary material Movie 1), possibly owing to the previously reported slow migration of distal cells (Vasilyev et al., 2009). The inhibited migration of the proximal

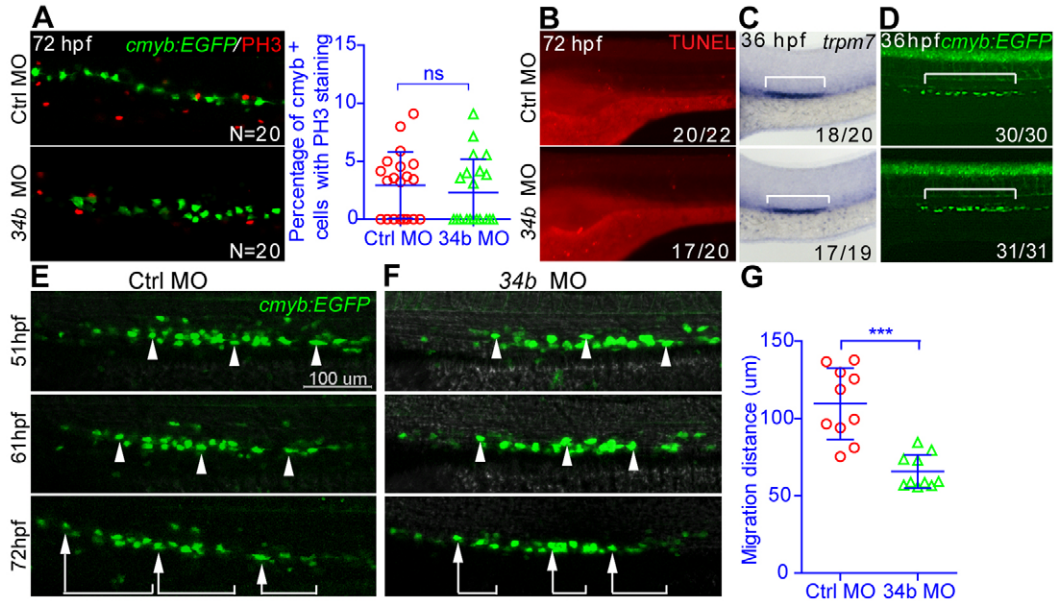

Fig. 3. MCC accumulation is mainly caused by attenuated cell migration. (**A**) A magnified lateral view of the kidney region after double staining of *cmyb:EGFP* and PH3 in 3-dpf embryos. (**B**) A magnified lateral view of the kidney region after TUNEL staining in 3-dpf embryos. (**C**,**D**) Distribution of transporting epithelial cells (bracket) (C) and MCCs (D) labeled by *trpm7* (WISH) and *Tg(cmyb:EGFP)* at 36 hpf. (B-D) The number of embryos with normal TUNEL staining, *trpm7* expression pattern or *cmyb* expression pattern among all analyzed embryos is indicated (bottom right). (**E-G**) The migration of MCCs labeled by *Tg(cmyb:EGFP)* from 51 to 72 hpf. Three representative MCCs were labeled (arrowheads and brackets) in embryos injected with either control (Ctrl) MO (E) or miR-34b MO (F). The migration distance of each MCC is shown in G (each circle/triangle represents an MCC, *n*=10). Mean ± s.d. ***P<0.0001 (unpaired *t*-test); ns, not significant. Scale bar: 100 μm.

MCCs towards the head kidney section might explain why the MCCs accumulated in the middle region of the pronephric ducts and suggests that miR-34b is important for the proper migration of MCCs during kidney morphogenesis.

miR-34b regulates kidney morphogenesis by controlling multiciliogenesis and fluid flow

To determine how miR-34b regulates the migration of MCCs and kidney morphogenesis, we isolated MCCs from the body section of *Tg(cmyb:EGFP)* fish at 3 dpf by FACS and performed microarray analysis on these cells (supplementary material Fig. S3A). The expression of 456 genes (of the 8296 examined) was changed more than 1.5-fold in MCCs of the miR-34b morphants (supplementary material Table S4), with 381 genes upregulated and 75 genes downregulated, when compared with MCCs from embryos injected with control MO. A GO enrichment analysis of these genes showed that cilium assembly and morphogenesis were among the processes most significantly affected in the miR-34b knockdown embryos (supplementary material Table S5). These include ciliary structural genes and genes involved in intraflagellar transport (Fig. 4A). The increased expression of these genes, along with key transcription factors for ciliogenesis such as *foxj1a*, *foxj1b* and *rfx2* (Bisgrove et al., 2012; Chung et al., 2012; Stubbs et al., 2008; Yu et al., 2008), was confirmed by QRT-PCR (Fig. 4B) and WISH (supplementary material Fig. S3B).

These results raised the possibility that multiciliogenesis might be affected in MCCs by miR-34b knockdown. We analyzed multiciliogenesis in MCCs by immunostaining with antibodies against acetylated tubulin, which is a major component of cilia, and EGFP, which marks *cmyb*-EGFP^{+} cells. At 30 hpf, the pronephric ducts in both the control animals and miR-34b morphants were filled with scattered single cilia (supplementary material Fig. S3C). However, at 36 hpf, when the cilia bundle was formed in each MCC in the control embryo, few cilia bundles were observed in the MCCs of the miR-34b morphants (Fig. 4C,D, arrows). By 2-3 dpf, the cilia bundles of the MCCs were aligned with the direction of fluid flow in the control embryo, whereas the thin and disorganized cilia bundles in the MCCs of miR-34b morphants were perpendicular to the fluid flow (supplementary material Fig. S3D, arrows). The single cilia in the proximal and distal ducts were, however, normal (supplementary material Fig. S3E, arrows). Furthermore, the cilia bundles in the olfactory placode did not form in the miR-34b morphants (Fig. 4E). On average, cilia were shorter in miR-34b morphants (2.3±0.3 μm) than in control animals (5.8±0.6 μm). These observations indicate that miR-34b plays essential roles in the formation and organization of cilia bundles in MCCs.

A previous report showed that the beating of cilia in the pronephric ducts drives directional fluid flow within the ducts (Kramer-Zucker et al., 2005). This led us to speculate that fluid flow might also be affected in miR-34b morphants. We analyzed fluid flow using a dye excretion assay (Fig. 4F). In accordance with the previous report, the time needed for excretion at the cloaca was 3.7±2.5 minutes in the control embryos. However, in miR-34b morphants the time needed more than doubled to 9.9±6.3 minutes (Fig. 4G), suggesting that fluid flow was severely affected. Another report showed that fluid flow is required for proximal tubule convolution and cell migration; blockage or irregularity of fluid flow results in defects in convolution and cell migration in the pronephric ducts (Vasilyev et al., 2009). Taken together, our results suggest that miR-34b regulates cilia bundles on MCCs, which are important for maintaining a steady fluid flow during kidney morphogenesis.

miR-34b regulates multiciliogenesis and kidney morphogenesis through *cmyb*

We next searched *in silico* prediction databases for putative miR-34b targets based on microarray data and the published literature (Hermeking, 2010). Ultimately, 24 genes (supplementary material Table S3) were tested for miR-34b regulation using an *in vivo*

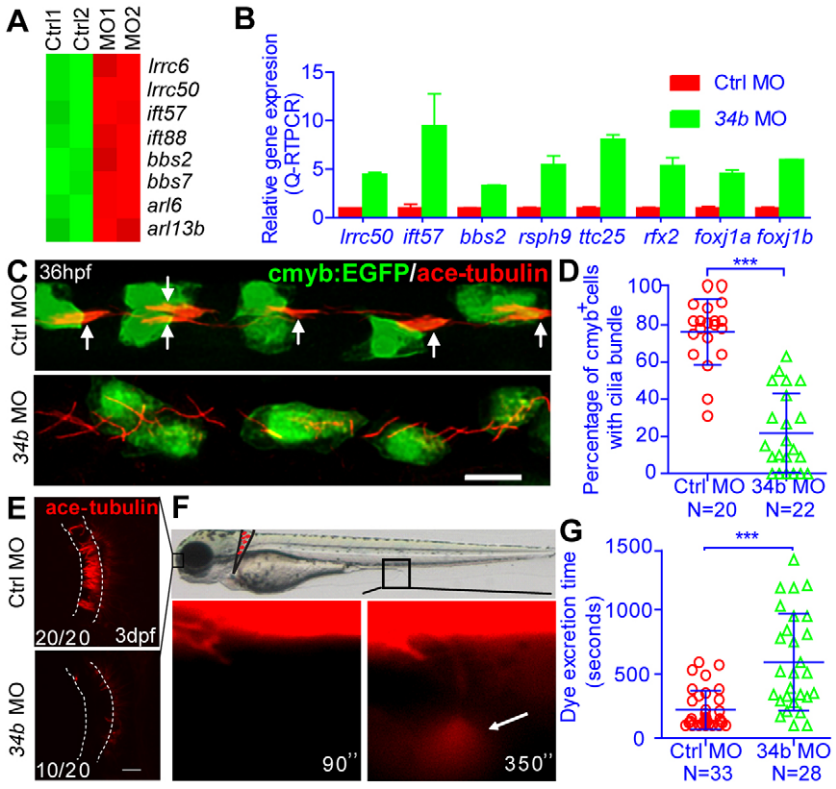

Fig. 4. miR-34b regulates kidney morphogenesis by controlling multiciliogenesis and fluid flow. (**A**) Heat map showing the expression of genes in the GO term Cilium Assembly. The color scale represents the expression level of a gene above (red) or below (green) the mean expression level across all samples. (**B**) QRT-PCR analysis of the expression of cilia genes in MCCs that were isolated from 3-dpf *Tg(cmyb:EGFP)* embryos by flow cytometry. The expression levels were normalized to that of β-*actin 1*. (**C**) The ciliary (anti-acetylated tubulin staining, red, arrows) morphology of the MCCs (anti-GFP staining, green) at 36 hpf in normal embryos and miR-34b morphants. Arrows indicate normal cilia bundles. (**D**) The percentage of *cmyb:EGFP*$^{+}$ cells with cilia bundles was calculated for each embryo and analyzed statistically at 36 hpf. (**E**) The ciliary morphology of the olfactory placode (outlined) at 3 dpf in normal embryos and miR-34b morphants. The number of embryos with normal cilia (top picture) or shorter cilia (bottom picture) among all analyzed embryos is indicated (bottom left). (**F**) Representative example of the dye excretion assay (3.5-dpf normal embryo), in which the time from injection until the first visible urine excretion at the cloaca (arrow) is measured. (**G**) Statistical analysis of the time from injection to dye excretion. Each circle/triangle represents an embryo. Mean ± s.d. ***P<0.0001 (unpaired t-test). Scale bar: 10 μm.

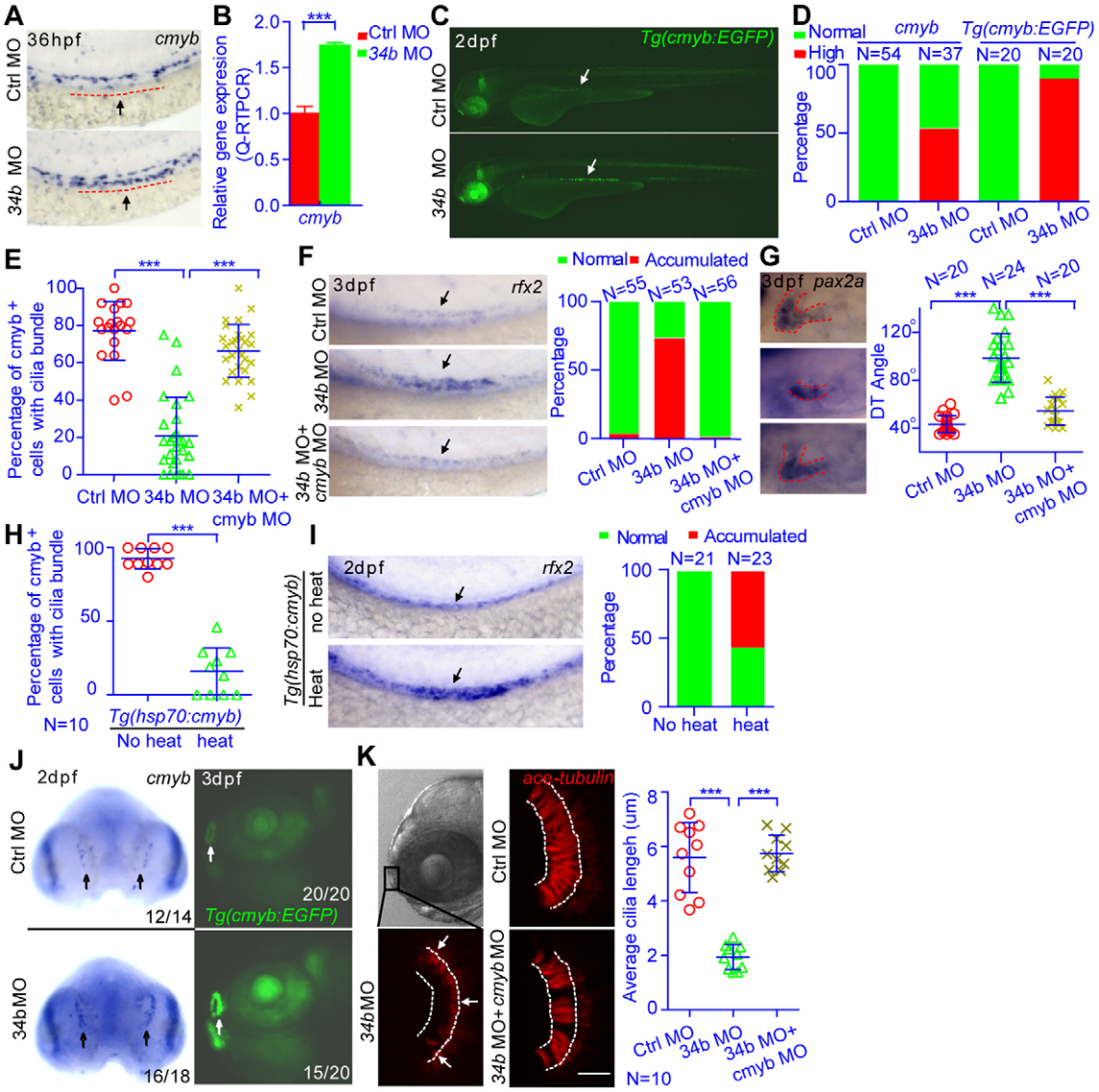

Fig. 5. miR-34b regulates multiciliogenesis and kidney morphogenesis through *cmyb*. (**A**) WISH analysis of *cmyb* expression at 36 hpf. The arrow and dashed line show the region of MCCs. (**B**) QRT-PCR analysis of *cmyb* expression in MCCs that were isolated from 3-dpf *Tg(cmyb:EGFP)* embryos by flow cytometry. The expression level was normalized to that of β-*actin 1*. (**C**) A 2-dpf *Tg(cmyb:EGFP)* embryo shows enhanced fluorescence in MCCs (arrow) after miR-34b knockdown. (**D**) Statistical analysis of A and C showing normal versus high expression of *cmyb*. (**E**) The percentage of *cmyb:EGFP*$^{+}$ cells with cilia bundles was calculated for each embryo and analyzed statistically at 36 hpf. (**F**,**G**) A magnified lateral view of 3-dpf embryos after *in situ* hybridization with *rfx2* or *pax2* probe shows the distribution of MCCs and the state of proximal tubule convolution. Arrows (F) indicate *rfx2*$^{+}$ MCCs. The DT angle was measured. (**H**) The percentage of *cmyb:EGFP*$^{+}$ cells with cilia bundles was calculated for each *Tg(hsp70:cmyb)* embryo and analyzed statistically at 36 hpf (**I**) A magnified lateral view of 2-dpf *Tg(hsp70:cmyb)* embryos after *in situ* hybridization with *rfx2* probe shows the distribution of MCCs. Arrows indicate *rfx2*$^{+}$ MCCs. The percentage of embryos with accumulated *rfx2*$^{+}$ MCCs (Accumulated) in F and I was calculated. (**J**) WISH analysis of *cmyb* expression at 2 dpf in the olfactory placode (arrows). A representative image of a 3-dpf *Tg(cmyb:EGFP)* embryo shows enhanced fluorescence of the olfactory placode (arrows) after miR-34b knockdown. The number of embryos with normal (top pictures) or high expression level (bottom pictures) of *cmyb* among all analyzed embryos is indicated (bottom right). (**K**) The ciliary (anti-acetylated-tubulin staining, red) morphology of the olfactory placode at 3 dpf in normal embryos, miR-34b morphants and embryos injected with both miR-34b MO and *cmyb* MO. Cilia length was analyzed at three positions (arrows) for each embryo, and the average cilia length is listed. Each circle/triangle/cross represents an embryo. Mean ± s.d. ***P<0.0001 (unpaired *t*-test). Scale bar: 10 μm.

reporter assay (Fu et al., 2009), in which either the predicted microRNA recognition sites (MREs) or the 3′ UTR was fused to *EGFP* and injected along with either a miR-34b duplex or control duplex. Transcripts of *cmyb* were upregulated 2-fold according to the microarray data, and the upregulation was confirmed both by QRT-PCR in FACS-isolated MCCs and by WISH analysis of whole embryos (Fig. 5A,B,D). We found two conserved miR-34b target sites in the 3′ UTR of *cmyb*. However, our reporter assay suggested that *cmyb* might not be a direct target of miR-34b (supplementary material Table S3). Enhanced fluorescence in the MCCs of *Tg(cmyb:EGFP)* embryos indicated that *cmyb* expression was regulated at the transcriptional level (Fig. 5C).

A previous report showed that *cmyb* function is required for multiciliogenesis in the subventricular zone of the brain (Malaterre

et al., 2008). During normal kidney development, expression of *cmyb* in MCCs begins at 24 hpf and decreases after 36 hpf, as monitored in the *Tg(cmyb:EGFP)* line (data not shown). We hypothesized that the upregulation of *cmyb* might play an important role in the defects caused by the inhibition of miR-34b function and predicted that normalization of *cmyb* expression levels in miR-34b morphants might rescue the cilia and kidney morphogenesis defects, whereas overexpression of *cmyb* alone should mimic the defects caused by reduced levels of miR-34b. When a series of 0.075 mM or 0.125 mM doses of *cmyb* MO were injected in combination with the miR-34b MO into *Tg(cmyb:EGFP)* embryos these treatments significantly rescued multiciliogenesis, MCC distribution and proximal tubule convolution (Fig. 5E-G). Overexpression of *cmyb* in *Tg(hsp70:cmyb)* zebrafish (Zhang et al., 2011) blocked cilia bundle formation and induced the accumulation of MCCs (Fig. 5H,I), similar to what was observed in the miR-34b morphants (Fig. 2; Fig. 4B). These results confirm that increased *cmyb* expression is directly responsible for the defective multiciliogenesis and abnormal kidney morphogenesis observed in miR-34b morphants.

We also found that *cmyb* was upregulated in the olfactory placode of miR-34b morphants (Fig. 5J). The injection of 0.125 mM *cmyb* MO together with the miR-34b MO rescued cilia bundle formation in the olfactory placode (Fig. 5K). These results show that the *miR-34b-cmyb* genetic pathway is required for multiciliogenesis in both the kidney and the olfactory organ during development.

The *miR-34b-cmyb* genetic pathway regulates the multiplication and membrane docking of centrioles

Multiciliogenesis begins with centriole multiplication in the cytoplasm, which is followed by membrane docking of the centrioles (Dawe et al., 2007). Using γ-tubulin as a centriole marker, we found tens to hundreds of centrioles scattered throughout the cytoplasm of MCCs at 24 hpf. At 30 hpf, centrioles began to aggregate in the cytoplasm and migrate to the cell surface in a fraction of MCCs. Most of the centrioles reached the cell surface by 36 hpf. However, in miR-34b morphants, most of the centrioles were retained in the cytoplasm until at least 48 hpf (Fig. 6A), indicating that the centrioles were unable to dock at the membrane. The injection of 0.125 mM *cmyb* MO together with the miR-34b MO rescued the centriole distribution defect in the MCCs of the kidney (Fig. 6A). These results suggest that the *miR-34b-cmyb* genetic pathway is required for the proper membrane docking of centrioles.

Genes involved in centriole formation, such as *plk4*, *stil*, *pcm1*, *nek2*, *poc1a* and *cep72*, were also more highly expressed in the MCCs of miR-34b morphants compared with control animals (Fig. 6C). *plk4* and *stil* play key roles in regulating centriole duplication (Brito et al., 2012). WISH analysis showed that *plk4* and *stil* are first expressed at ~24 hpf in MCCs, were downregulated from 30 hpf and were not detected at 36 hpf (Fig. 6D; Fig. 7F). This expression pattern is consistent with the timing of centriole multiplication, indicating that *plk4* and *stil* might play important roles during centriole multiplication. However, in the miR-34b morphants, expression of *plk4* and *stil* was maintained at a high level until at least 36 hpf (Fig. 6D,E). These results suggest that there is a prolonged centriole multiplication period in miR-34b morphants.

Next, we tested how *cmyb* is involved in miR-34b-regulated centriole multiplication by performing loss- and gain-of-function analyses using the *cmyb*^{hkz3} mutant (Zhang et al., 2011) and the *hsp70:cmyb* transgenic line. In the middle section of the kidney duct fewer MCCs had membrane-docking centrioles in *cmyb* mutants than in wild-type embryos (Fig. 7A,C). Accordingly, fewer cilia bundles with organized structures were observed in the *cmyb*

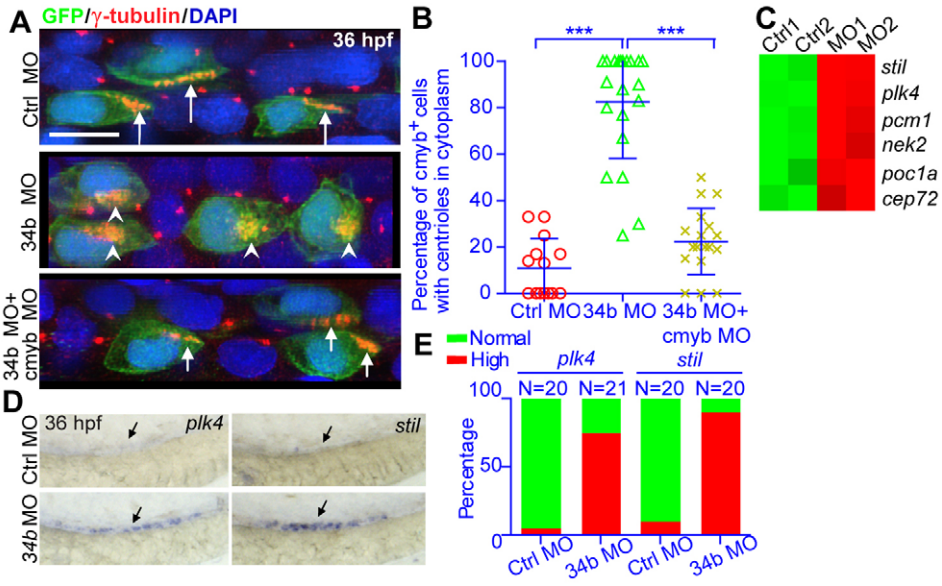

Fig. 6. *The miR-34b-cmyb* genetic pathway regulates the multiplication and membrane docking of centrioles. (**A**) The centriole (anti-γ-tubulin staining, red, arrows) morphology of MCCs (anti-GFP staining, green) in normal embryos, miR-34b morphants and embryos injected with both miR-34b MO and *cmyb* MO. Arrows indicate centrioles on the cell surface; arrowheads indicate centrioles in the cytoplasm. (**B**) Statistical analysis of A. Each circle/triangle/cross represents an embryo. Mean ± s.d. ***P<0.0001 (unpaired t-test). (**C**) Heat map showing the expression of genes related to centriole duplication from the microarray data of 3-dpf MCCs. The color scale represents the expression level of a gene above (red) or below (green) the mean expression level across all samples. (**D**) WISH analysis of *plk4* and *stil* expression at 36 hpf. The arrow identifies the appropriate MCC region. (**E**) Statistical analysis of D showing normal versus high expression of *plk4* and *stil*.

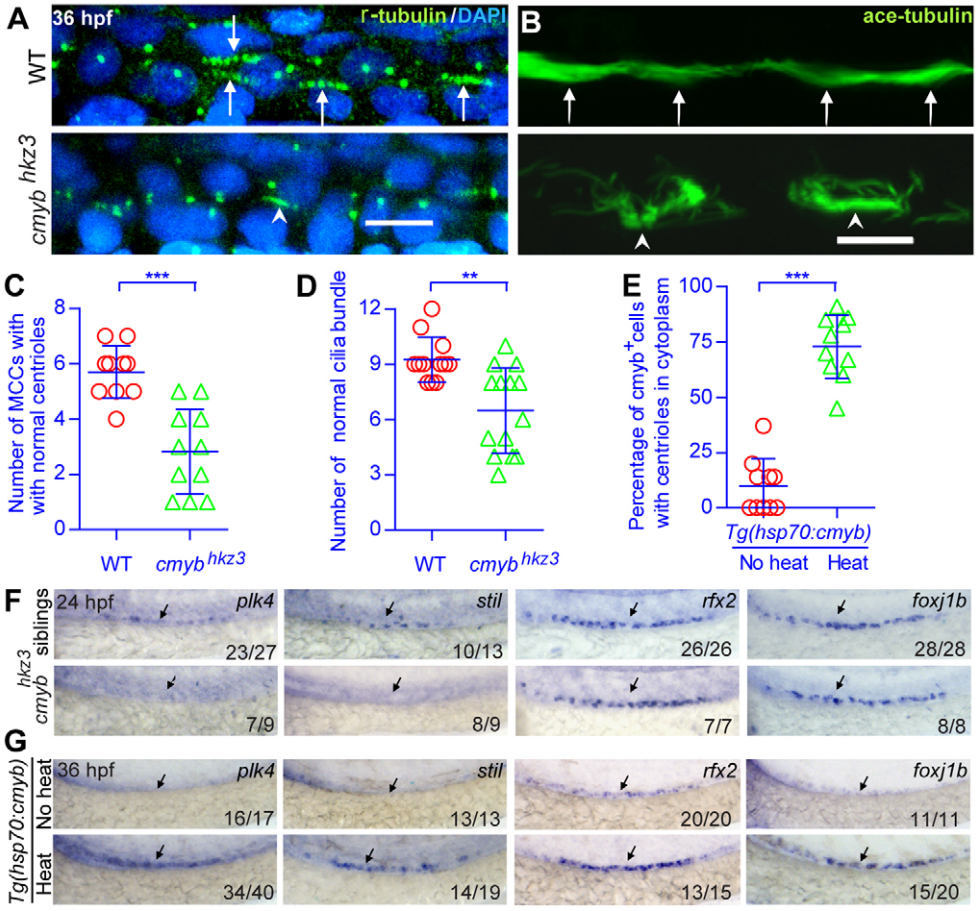

Fig. 7. *cmyb* regulates the expression of key regulatory genes involved in centriole duplication and ciliogenesis. (**A-D**) Morphological and statistical analysis of the centriole (anti-γ-tubulin staining, green in A) and cilia bundle (anti-acetylated tubulin staining, green in B) in the middle kidney duct of wild-type and *cmyb* mutant embryos. Membrane RFP was injected and stained to help identify the cell boundaries (data not shown). Arrows indicate normal centrioles and ciliar bundles; arrowheads indicate defective centrioles and cilia bundles. (**E**) The percentage of *cmyb:EGFP*$^{+}$ cells with cilia bundles was calculated for each *Tg(hsp70:cmyb)* embryo and analyzed statistically at 36 hpf. (C-E) Each circle/triangle represents an embryo. Mean ± s.d. $^{**}P<0.01$, $^{***}P<0.0001$ (unpaired *t*-test). (**F**,**G**) WISH analysis of *plk4*, *stil*, *rfx2* and *foxj1b* expression in normal embryos, *cmyb* mutants and embryos overexpressing *cmyb*. Arrows indicate the regions where MCCs are located. The number of embryos with normal (top pictures in F,G), low (bottom pictures in F) or high expression levels (bottom pictures in G) of a tested gene among all analyzed embryos is indicated (bottom right). WT, wild type. Scale bars: 10 μm.

mutants (Fig. 7B,D). Loss of *cmyb* also resulted in the downregulation of *plk4* and *stil*, but not of *foxj1b* or *rfx2*. Conversely, overexpression of *cmyb* blocked the membrane docking of centrioles and induced a profound and specific upregulation of *plk4*, *stil*, *rfx2* and *foxj1b* in kidney MCCs, consistent with the results from the miR-34b morphants (Fig. 7E-G) and suggesting that *cmyb* participates in the regulation of multiciliogenesis by controlling the key transcriptional regulators of centriole multiplication. These results suggested that an optimal level of *cmyb* expression is required for both centriole multiplication and multiciliogenesis.

DISCUSSION

Proximal tubule convolution and distal cell migration are important for the formation of a functional kidney in zebrafish. A previous report showed that fluid flow driven by blood pressure and cilia is essential for this process (Vasilyev et al., 2009). Here, we show that proper multiciliogenesis of MCCs is required for kidney morphogenesis and identify the *miR-34b-cmyb* axis as an important genetic pathway in the regulation of this process. miR-34b was preferentially expressed in MCCs and may indirectly suppress *cmyb* expression, permitting normal multiciliogenesis, fluid flow and kidney cell migration. The *miR-34b-cmyb* genetic pathway controls the multiplication and membrane docking of centrioles during multiciliogenesis, providing new insight into the molecular regulation of this key process. The *miR-34b-cmyb* genetic pathway is also required for multiciliogenesis in the olfactory placode. Because miR-34b is specifically expressed in MCC-enriched tissues in human and *Xenopus* (Hsu et al., 2008; Liang, 2008; Marcet et al., 2011), it is likely that the *miR-34b-cmyb* genetic pathway is evolutionarily conserved and widely used for the control of multiciliogenesis. This finding has improved our understanding of fluid flow control, organ morphogenesis and multiciliogenesis.

Regulation of fluid flow during organogenesis and tissue development

Fluid flow and fluid shear forces are important during organogenesis and tissue development. In a cilia-driven fluid system, the proper distribution of cilia along the duct (channel) is essential for constant fluid flow. However, the underlying mechanisms and functional importance of cilia distribution during development are not well understood. In zebrafish, the pronephric duct is filled with both scattered single cilia (proximal and distal ducts) and organized cilia bundles (middle ducts) (Kramer-Zucker et al., 2005; Liu et al., 2007; Ma and Jiang, 2007; Sullivan-Brown et al., 2008). miR-34b was preferentially expressed in MCCs, and knockdown of miR-34b specifically blocked the formation and maintenance of the cilia bundles without disturbing the single cilia, thus revealing the essential function of the cilia bundles in the middle ducts.

The major difference between miR-34b morphants and other cilia mutants is the lack of cyst formation in the anterior kidney (Sullivan-Brown et al., 2008). This result is also consistent with a previous report on the cyst-inducing mutant *kurly*, which displays kidney cysts and impaired single cilia, but normal cilia bundles (Sullivan-Brown et al., 2008). These results suggest that single cilia play an important role in cyst formation at the anterior kidney, whereas cilia bundles do not. According to mammalian kidney cyst models, the sensory role of the primary cilia is important during

cyst formation (Chapin and Caplan, 2010), raising the question of whether the single cilia in the zebrafish kidney duct have a sensory function. Our results show that the proper distribution of single cilia and cilia bundles during organogenesis is important for correct fluid control and organogenesis. The principles that regulate cilia formation and distribution merit further research.

Molecular regulation of multiciliogenesis

Although many signaling pathways and molecules play key roles in regulating primary cilia or single motile cilia, few are known to be important in the molecular control of multiciliogenesis. In our studies, we found that an optimal level of *cmyb* expression is crucial for proper multiciliogenesis. Higher expression levels of *cmyb* block the membrane docking of centrioles, whereas loss of *cmyb* impairs centriole multiplication, and both result in defects in cilia bundle formation and organization. miR-34b serves as a guardian to maintain optimal levels of *cmyb*. Further studies will utilize RIP-ChIP to provide insight into the targets of miR-34b and discover how it is involved in maintaining the level of *cmyb* in MCCs (Nelson et al., 2010; Thomson et al., 2011). We found that *plk4* and *stil* were preferentially expressed in MCCs during centriole multiplication and were upregulated after miR-34b knockdown. Loss- and gain-of-function studies showed that *cmyb* is genetically upstream of *plk4* and *stil*, which thus participate in the process of centriole multiplication. How *plk4* and *stil* participate in centriole multiplication deserves further research.

We observed the upregulation of ciliary genes, including *rfx2* and *foxj1a*, in miR-34b morphants, which is consistent with previous reports on cilia mutants. This upregulation is correlated with pronephric duct dilation, which is induced by a stretching force (Hellman et al., 2010). In the miR-34b morphants we observed similar tubule dilation (Fig. 2I,J), consistent with the upregulation of these cilia genes. The upregulated ciliary genes could also reflect a state of incomplete multiciliogenesis resulting from the blockage of centriole membrane docking, suggesting that the processes of centriole multiplication and ciliogenesis are closely connected. Further research is required to illustrate how these two processes are related.

miR-34b and cancer

miR-34b regulates the proliferation, apoptosis and migration of cancer cells by intersecting with p53 signaling (He et al., 2007; Hermeking, 2010). In our analysis, we did not observe any changes in cell proliferation, apoptosis or in the components of the p53 pathway in the miR-34b morphants, which might be because MCCs were not in a proliferative state. However, we did discover a link between miR-34b and centriole multiplication. It will be interesting to determine whether this centriole duplication defect is involved in miR-34b-related cancer. In addition, a recent study showed that primary cilia play an important role in tumorigenesis (Hassounah et al., 2012). Our results also raise the question of whether miR-34b contributes to cilia-related cancers, especially in tissues with MCCs.

Acknowledgements

We thank Dr Len Zon at Harvard Medical School for providing the *Tg(cmyb:EGFP)* line. Dr Yiyue Zhang at Southern Medical University (China) provided the *Tg(hsp70:cmyb)* and *cmyb*^{hkz3} lines; Song Guo and Haiyang Hu of Dr Philipp Khaitovich's group at CAS-MPG Partner Institute helped with the microarray analysis; Dr Lihui Lai at East China Normal University helped with microRNA target identification; and Drs Anming Meng at Tsinghua University, Iain A. Drummond at Massachusetts General Hospital and Laure Bally-Cuif at CNRS provided WISH plasmids. We thank Dr Weijun Pan and all members of the laboratory for helpful discussions.

Funding

This work was supported by the National Basic Research Program of China [2007CB947003]; the Strategic Priority Research Program of the Chinese Academy of Science [XDA 01010109]; and the National Natural Science Foundation of China [30830047, 31000636].

Competing interests statement

The authors declare no competing financial interests.

Author contributions

L.W. and C.F. performed experiments and analyzed data; H.F., T.D., M. Dong, Y.C. and Y.J. assisted with experiments; L.W., M. Deng, Yi Zhou, A.G., Q.J., T.L. and Yong Zhou designed the research plan; and L.W., Yi Zhou, A.G., Q.J. and Yong Zhou wrote the paper.

Supplementary material

Supplementary material available online at
http://dev.biologists.org/lookup/suppl/doi:10.1242/dev.092825/-/DC1

References

Abu-Issa, R. and Kirby, M. L. (2007). Heart field: from mesoderm to heart tube. *Annu. Rev. Cell Dev. Biol.* **23**, 45-68.

Agostini, M., Tucci, P., Killick, R., Candi, E., Sayan, B. S., Rivetti di Val Cervo, P., Nicotera, P., McKeon, F., Knight, R. A., Mak, T. W. et al. (2011a). Neuronal differentiation by TAp73 is mediated by microRNA-34a regulation of synaptic protein targets. *Proc. Natl. Acad. Sci. USA* **108**, 21093-21098.

Agostini, M., Tucci, P., Steinert, J. R., Shalom-Feuerstein, R., Rouleau, M., Aberdam, D., Forsythe, I. D., Young, K. W., Ventura, A., Concepcion, C. P. et al. (2011b). microRNA-34a regulates neurite outgrowth, spinal morphology, and function. *Proc. Natl. Acad. Sci. USA* **108**, 21099-21104.

Bertrand, J. Y., Kim, A. D., Teng, S. and Traver, D. (2008). CD41+ cmyb+ precursors colonize the zebrafish pronephros by a novel migration route to initiate adult hematopoiesis. *Development* **135**, 1853-1862.

Bisgrove, B. W., Makova, S., Yost, H. J. and Brueckner, M. (2012). RFX2 is essential in the ciliated organ of asymmetry and an RFX2 transgene identifies a population of ciliated cells sufficient for fluid flow. *Dev. Biol.* **363**, 166-178.

Bouhallier, F., Allioli, N., Lavial, F., Chalmel, F., Perrard, M. H., Durand, P., Samarut, J., Pain, B. and Rouault, J. P. (2010). Role of miR-34c microRNA in the late steps of spermatogenesis. *RNA* **16**, 720-731.

Brend, T. and Holley, S. A. (2009). Zebrafish whole mount high-resolution double fluorescent in situ hybridization. *J. Vis. Exp.* **25**, 1229.

Brito, D. A., Gouveia, S. M. and Bettencourt-Dias, M. (2012). Deconstructing the centriole: structure and number control. *Curr. Opin. Cell Biol.* **24**, 4-13.

Chapin, H. C. and Caplan, M. J. (2010). The cell biology of polycystic kidney disease. *J. Cell Biol.* **191**, 701-710.

Chung, M. I., Peyrot, S. M., LeBoeuf, S., Park, T. J., McGary, K. L., Marcotte, E. M. and Wallingford, J. B. (2012). RFX2 is broadly required for ciliogenesis during vertebrate development. *Dev. Biol.* **363**, 155-165.

Dawe, H. R., Farr, H. and Gull, K. (2007). Centriole/basal body morphogenesis and migration during ciliogenesis in animal cells. *J. Cell Sci.* **120**, 7-15.

Dressler, G. R. (2006). The cellular basis of kidney development. *Annu. Rev. Cell Dev. Biol.* **22**, 509-529.

Drummond, I. A. (2005). Kidney development and disease in the zebrafish. *J. Am. Soc. Nephrol.* **16**, 299-304.

Drummond, I. A. and Davidson, A. J. (2010). Zebrafish kidney development. *Methods Cell Biol.* **100**, 233-260.

Ebarasi, L., Oddsson, A., Hultenby, K., Betsholtz, C. and Tryggvason, K. (2011). Zebrafish: a model system for the study of vertebrate renal development, function, and pathophysiology. *Curr. Opin. Nephrol. Hypertens.* **20**, 416-424.

Ewald, A. J., Brenot, A., Duong, M., Chan, B. S. and Werb, Z. (2008). Collective epithelial migration and cell rearrangements drive mammary branching morphogenesis. *Dev. Cell* **14**, 570-581.

Fliegauf, M., Benzing, T. and Omran, H. (2007). When cilia go bad: cilia defects and ciliopathies. *Nat. Rev. Mol. Cell Biol.* **8**, 880-893.

Freund, J. B., Goetz, J. G., Hill, K. L. and Vermot, J. (2012). Fluid flows and forces in development: functions, features and biophysical principles. *Development* **139**, 1229-1245.

Fu, Y. F., Du, T. T., Dong, M., Zhu, K. Y., Jing, C. B., Zhang, Y., Wang, L., Fan, H. B., Chen, Y., Jin, Y. et al. (2009). Mir-144 selectively regulates embryonic alpha-hemoglobin synthesis during primitive erythropoiesis. *Blood* **113**, 1340-1349.

Hall, C., Flores, M. V., Crosier, K. and Crosier, P. (2009). Live cell imaging of zebrafish leukocytes. *Methods Mol. Biol.* **546**, 255-271.

Hassounah, N. B., Bunch, T. A. and McDermott, K. M. (2012). Molecular pathways: the role of primary cilia in cancer progression and therapeutics with a focus on Hedgehog signaling. *Clin. Cancer Res.* **18**, 2429-2435.

He, L., He, X., Lowe, S. W. and Hannon, G. J. (2007). microRNAs join the p53 network—another piece in the tumour-suppression puzzle. *Nat. Rev. Cancer* **7**, 819-822.
Hellman, N. E., Liu, Y., Merkel, E., Austin, C., Le Corre, S., Beier, D. R., Sun, Z., Sharma, N., Yoder, B. K. and Drummond, I. A. (2010). The zebrafish foxj1a transcription factor regulates cilia function in response to injury and epithelial stretch. *Proc. Natl. Acad. Sci. USA* **107**, 18499-18504.
Hermeking, H. (2010). The miR-34 family in cancer and apoptosis. *Cell Death Differ.* **17**, 193-199.
Hildebrandt, F., Benzing, T. and Katsanis, N. (2011). Ciliopathies. *N. Engl. J. Med.* **364**, 1533-1543.
Hsu, S. D., Chu, C. H., Tsou, A. P., Chen, S. J., Chen, H. C., Hsu, P. W., Wong, Y. H., Chen, Y. H., Chen, G. H. and Huang, H. D. (2008). miRNAMap 2.0: genomic maps of microRNAs in metazoan genomes. *Nucleic Acids Res.* **36**, D165-D169.
Huang, W., Sherman, B. T. and Lempicki, R. A. (2009). Systematic and integrative analysis of large gene lists using DAVID bioinformatics resources. *Nat. Protoc.* **4**, 44-57.
Kamei, M. and Weinstein, B. M. (2005). Long-term time-lapse fluorescence imaging of developing zebrafish. *Zebrafish* **2**, 113-123.
Kramer-Zucker, A. G., Olale, F., Haycraft, C. J., Yoder, B. K., Schier, A. F. and Drummond, I. A. (2005). Cilia-driven fluid flow in the zebrafish pronephros, brain and Kupffer's vesicle is required for normal organogenesis. *Development* **132**, 1907-1921.
Lehtinen, M. K., Zappaterra, M. W., Chen, X., Yang, Y. J., Hill, A. D., Lun, M., Maynard, T., Gonzalez, D., Kim, S., Ye, P. et al. (2011). The cerebrospinal fluid provides a proliferative niche for neural progenitor cells. *Neuron* **69**, 893-905.
Liang, Y. (2008). An expression meta-analysis of predicted microRNA targets identifies a diagnostic signature for lung cancer. *BMC Med. Genomics* **1**, 61.
Liu, Y., Pathak, N., Kramer-Zucker, A. and Drummond, I. A. (2007). Notch signaling controls the differentiation of transporting epithelia and multiciliated cells in the zebrafish pronephros. *Development* **134**, 1111-1122.
Liu, W. M., Pang, R. T., Chiu, P. C., Wong, B. P., Lao, K., Lee, K. F. and Yeung, W. S. (2012). Sperm-borne microRNA-34c is required for the first cleavage division in mouse. *Proc. Natl. Acad. Sci. USA* **109**, 490-494.
Ma, M. and Jiang, Y. J. (2007). Jagged2a-notch signaling mediates cell fate choice in the zebrafish pronephric duct. *PLoS Genet.* **3**, e18.
Malaterre, J., Mantamadiotis, T., Dworkin, S., Lightowler, S., Yang, Q., Ransome, M. I., Turnley, A. M., Nichols, N. R., Emambokus, N. R., Frampton, J. et al. (2008). c-Myb is required for neural progenitor cell proliferation and maintenance of the neural stem cell niche in adult brain. *Stem Cells* **26**, 173-181.
Malicki, J., Avanesov, A., Li, J., Yuan, S. and Sun, Z. (2011). Analysis of cilia structure and function in zebrafish. *Methods Cell Biol.* **101**, 39-74.
Marcet, B., Chevalier, B., Luxardi, G., Coraux, C., Zaragosi, L. E., Cibois, M., Robbe-Sermesant, K., Jolly, T., Cardinaud, B., Moreilhon, C. et al. (2011). Control of vertebrate multiciliogenesis by miR-449 through direct repression of the Delta/Notch pathway. *Nat. Cell Biol.* **13**, 693-699.
Nelson, P. T., Kiriakidou, M., Mourelatos, Z., Tan, G. S., Jennings, M. H., Xie, K. and Wang, W. X. (2010). High-throughput experimental studies to identify miRNA targets directly, with special focus on the mammalian brain. *Brain Res.* **1338**, 122-130.
North, T. E., Goessling, W., Walkley, C. R., Lengerke, C., Kopani, K. R., Lord, A. M., Weber, G. J., Bowman, T. V., Jang, I. H., Grosser, T. et al. (2007). Prostaglandin E2 regulates vertebrate haematopoietic stem cell homeostasis. *Nature* **447**, 1007-1011.
Poelmann, R. E., Gittenberger-de Groot, A. C. and Hierck, B. P. (2008). The development of the heart and microcirculation: role of shear stress. *Med. Biol. Eng. Comput.* **46**, 479-484.
Si-Tayeb, K., Lemaigre, F. P. and Duncan, S. A. (2010). Organogenesis and development of the liver. *Dev. Cell* **18**, 175-189.
Soza-Ried, C., Hess, I., Netuschil, N., Schorpp, M. and Boehm, T. (2010). Essential role of c-myb in definitive hematopoiesis is evolutionarily conserved. *Proc. Natl. Acad. Sci. USA* **107**, 17304-17308.
Stubbs, J. L., Oishi, I., Izpisúa Belmonte, J. C. and Kintner, C. (2008). The forkhead protein Foxj1 specifies node-like cilia in Xenopus and zebrafish embryos. *Nat. Genet.* **40**, 1454-1460.
Sullivan-Brown, J., Schottenfeld, J., Okabe, N., Hostetter, C. L., Serluca, F. C., Thiberge, S. Y. and Burdine, R. D. (2008). Zebrafish mutations affecting cilia motility share similar cystic phenotypes and suggest a mechanism of cyst formation that differs from pkd2 morphants. *Dev. Biol.* **314**, 261-275.
Thomson, D. W., Bracken, C. P. and Goodall, G. J. (2011). Experimental strategies for microRNA target identification. *Nucleic Acids Res.* **39**, 6845-6853.
Vasilyev, A., Liu, Y., Mudumana, S., Mangos, S., Lam, P. Y., Majumdar, A., Zhao, J., Poon, K. L., Kondrychyn, I., Korzh, V. et al. (2009). Collective cell migration drives morphogenesis of the kidney nephron. *PLoS Biol.* **7**, e9.
Wienholds, E., Kloosterman, W. P., Miska, E., Alvarez-Saavedra, E., Berezikov, E., de Bruijn, E., Horvitz, H. R., Kauppinen, S. and Plasterk, R. H. (2005). MicroRNA expression in zebrafish embryonic development. *Science* **309**, 310-311.
Yu, X., Ng, C. P., Habacher, H. and Roy, S. (2008). Foxj1 transcription factors are master regulators of the motile ciliogenic program. *Nat. Genet.* **40**, 1445-1453.
Zhang, Y., Jin, H., Li, L., Qin, F. X. and Wen, Z. (2011). cMyb regulates hematopoietic stem/progenitor cell mobilization during zebrafish hematopoiesis. *Blood* **118**, 4093-4101.

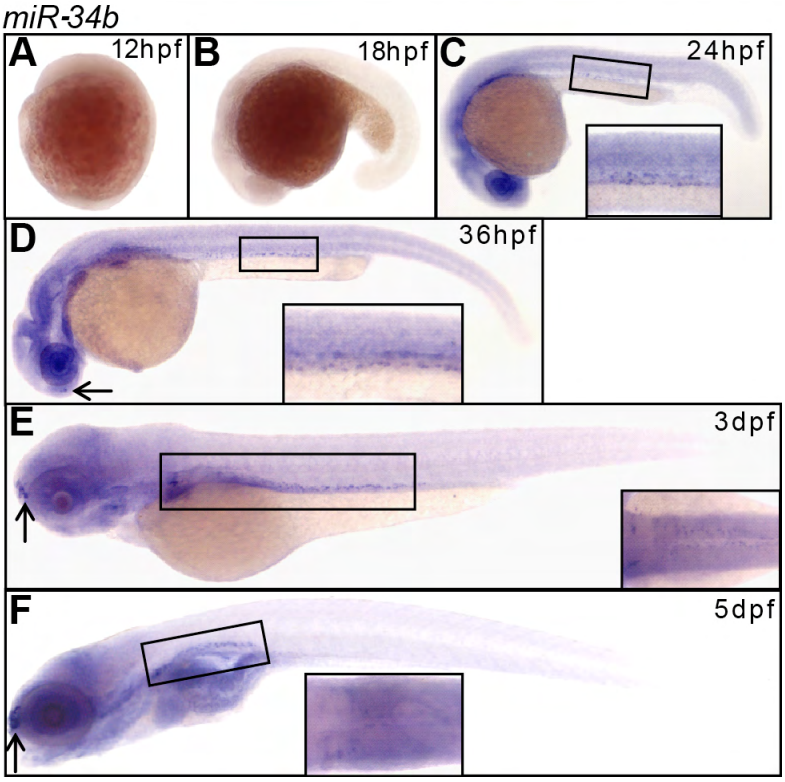

Fig. S1. Expression pattern of miR-34b (WISH) during development. (**A-F**) Expression of miR-34b is first observed at 24 hpf (C) at the kidney region and persists until at least 5 dpf (F). Magnified lateral view with a small angle to dorsal shows that the labeled cells reside in both pronephric ducts (C,D, insets). Magnified dorsal view (E,F) of the kidney region is shown in the inset. Olfactory placode is indicated by arrows.

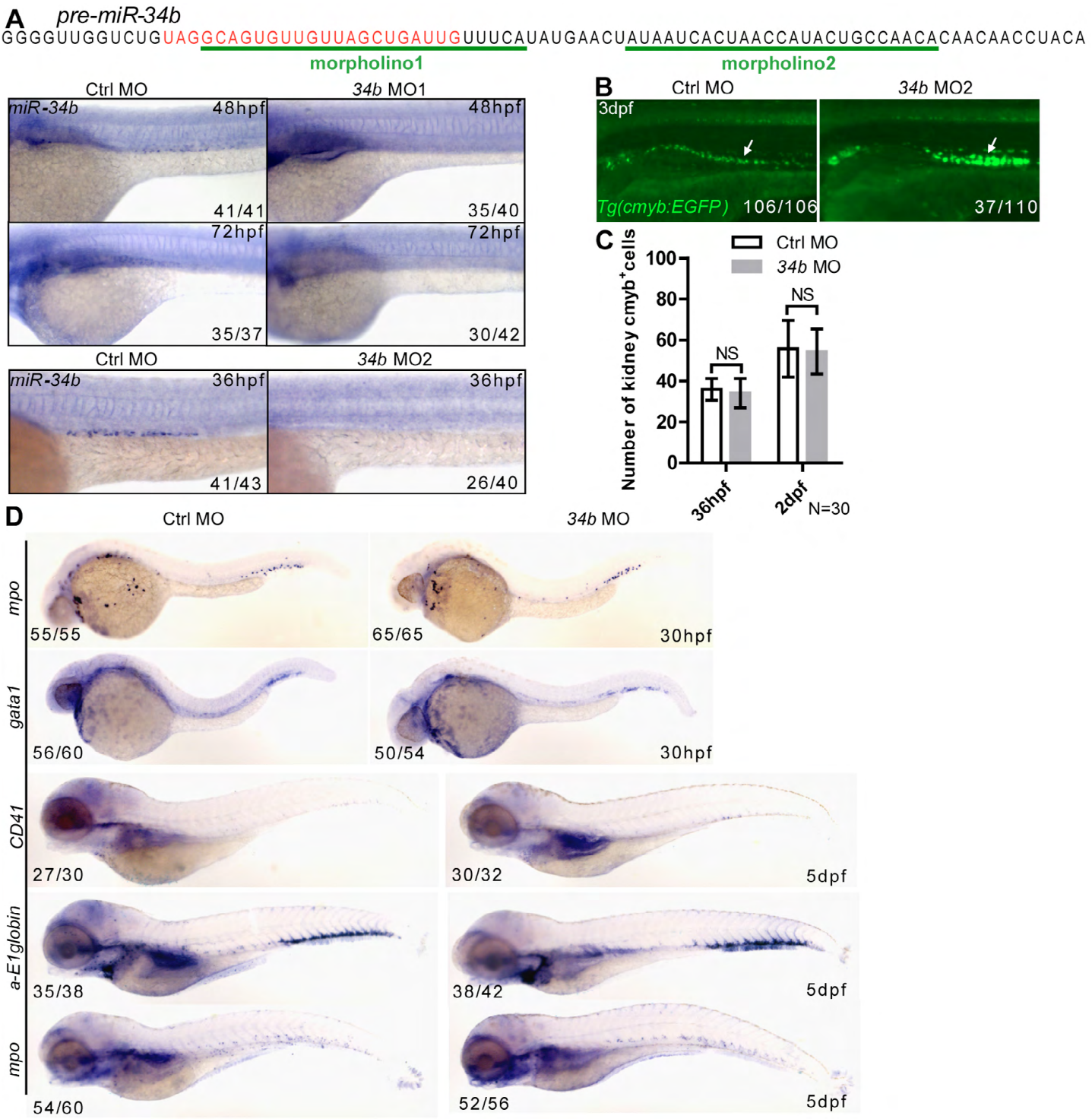

Fig. S2. Successful knockdown of miR-34b by morpholinos. (**A**) Two morpholinos were designed and shown to block the biogenesis of mature miR-34b (WISH). (**B**) Image of *Tg(cmyb:EGFP)* embryo shows that MCCs accumulate in the middle part of pronephric duct at 3 dpf after miR-34b MO2 injection. (**C**) Manual count of MCCs labeled by *Tg(cmyb:EGFP)* at 36 and 48 hpf. *n*=30 for Ctrl MO and miR-34b MO (mean ± s.d.). (**D**) Representative results show hematopoiesis after miR-34b knockdown.

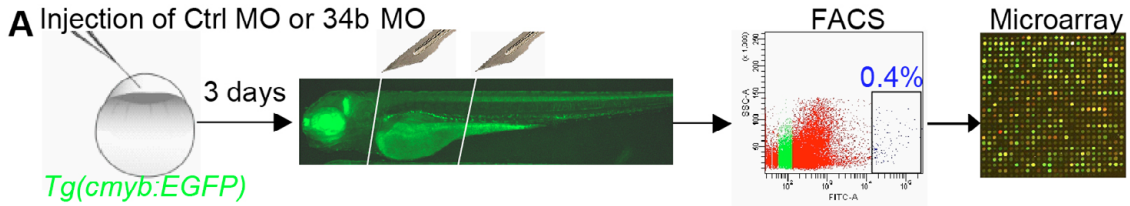

Go Term	Count	%	Fold Enrichment	P-value
cilium assembly	8	2.1	19.8	7.9E-08
microtubule-based process	13	3.4	7.6	10.0E-08
cell projection assembly	9	2.3	14.0	1.6E-07
cilium morphogenesis	8	2.1	167	2.9E-07
cell projection organization	11	2.8	5.2	4.3E-05

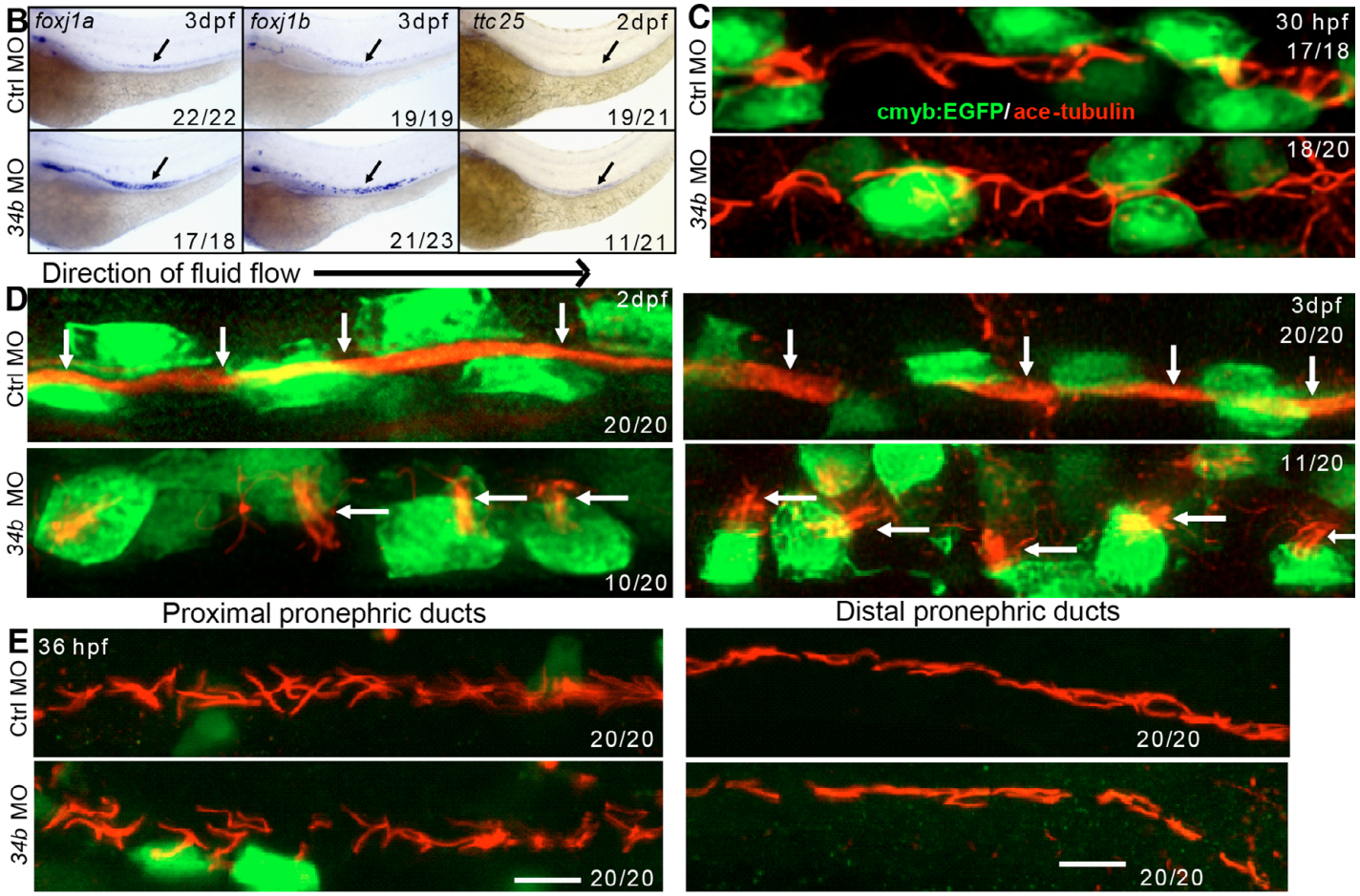

Fig. S3. Analysis of MCC gene expression profile and multiciliogenesis. (**A**) Work flow of microarray analysis. (**B**) Expression analysis of upregulated ciliary genes in the microarray data by WISH. (**C**,**D**) The ciliary morphology (anti-acetylated tubulin staining, red, arrows) of MCCs (anti-GFP staining, green) at 30 hpf (C), 2 dpf and 3 dpf (D) in normal embryos and miR-34b morphants. (**E**) The ciliary morphology (red) at proximal and distal pronephric ducts of 36-hpf normal embryos and miR-34b morphants.

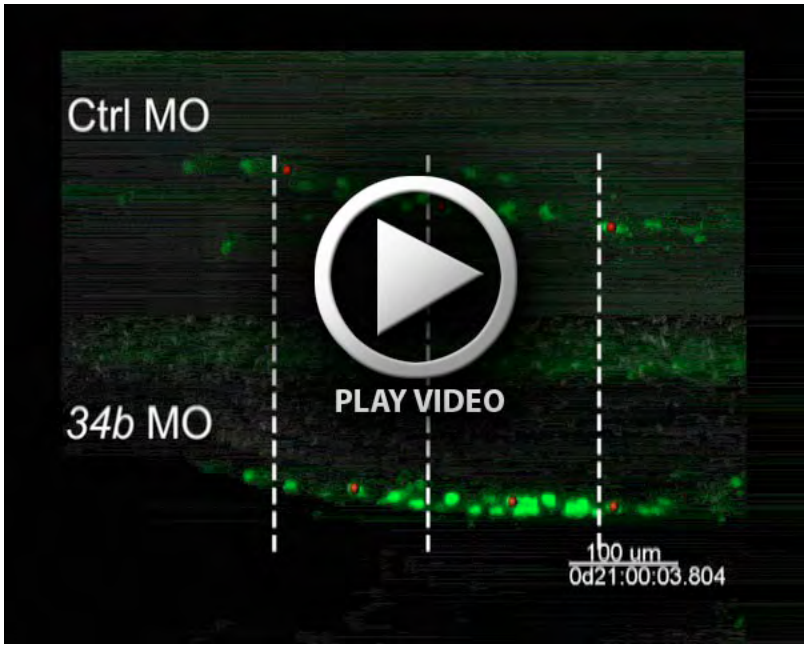

Movie 1. The migration of MCCs labeled by *Tg(cmyb:EGFP)* from 51 to 72 hpf. Three representative MCCs were labeled (red spots) in embryos injected with Ctrl MO (up) or miR-34b MO (down) using image analysis software; each embryo was captured independently and combined (see Materials and methods).

Table S1. Morpholino and duplex sequences

Name	Sequence	Dose	Reference
34b MO1	TGAAACAATCAGCTAACAACACTGC	1 mM	This paper
34b MO2	TGTTGGCAGTATGGTTAGTGATTAT	0.25 mM	This paper
Ctrl MO	CCTCTTACCTCAGTTACAATTTATA	1 mM	This paper
rfx2 MO	GGGTGTAGTCTGACCTGGTAC	0.25 mM	Liu et al., 2007
rfx2 MO	GGGTGTAGTCTGACCTGGTAC	0.0625/0.125 mM (rescue)	Liu et al., 2007
hoxb8a MO	AGCTCATCTTTTACTGCTGTTGGTG	0.5 mM (knockdown)	This paper
hoxb8a MO	AGCTCATCTTTTACTGCTGTTGGTG	0.375 mM (rescue)	This paper
cmyb MO	TCGCCATCCCGCTGTTCGAGAGGAA	0.125 mM (knockdown)	Soza-Ried et al., 2010
cmyb MO	TCGCCATCCCGCTGTTCGAGAGGAA	0.075/0.125 mM (rescue)	Soza-Ried et al., 2010
34b duplex F	UAGGCAGUGUUGUUAGCUGAUUGdTdT	10 μM	This paper
34b duplex R	CAAUCAGCUAACAACACUGCCAAdTdT	10 μM	This paper
Ctrl duplex F	CCAGGGAUUUCAGUCGAUGUAdTdT	10 μM	This paper
Ctrl duplex R	UACAUCGACUGAAAUCCCUCGdTdT	10 μM	This paper

Table S2. QRT-PCR primer sequences

Gene	Primer sequence (forward/reverse)
rfx2	CCGGAGATCATCAGCACTAAGG/GGTCGCTGAGCATCTGATTGA
foxj1a	TACTTCCGCCACGCAGAT/GGGTCGATTTTCCAGAAGC
foxj1b	CGTGAAGCCACCCTATTCAT/GGATTGAGTTCTGCCAGCTC
ttc25	ACGCCGAGAGCTCACTTAAA/AACTCAAAATCGCCCATAGTGT
ift57	GATGCCAAGGGTTGTCTGTT/GCTCCTTCACCTTGTTGAGC
bbs2	GAACCCACTGGAAAAGTCACA/ACGTCTGGACTGTCGATGC
rsph9	TGATGAACTGAAGAACAGGAAGTC/CATCTGCAATCATGGACTCG
lrrc50	CGTATCCACATCGATGAACG/AGCAGCTGCACTCTGAGAATC
cmyb	TGATGCTTCCCAACACAGAG/TTCAGAGGGAATCGTCTGCT
β-*actin 1*	CGAGCAGGAGATGGGAACC/CAACGGAAACGCTCATTGC

Table S3. Target identification by 2×MRE and UTR reporter assay

Name	Sequence	Response to miR-34b mimic
cdk6 MRE	UGUUCAGUUCACCACACUGCCAG	No
taf5 MRE	AUACAAGCUUUUAUACUACUGCCUA	Yes
strap MRE	UAAUGCUAAUCCUCCAGCUGCCUG	No
mycb MRE	CAAUUCACACUGCCUC	Yes
skap2 MRE	UAAUACGUAAAGCAAACUGCCUG	Yes
znf395 MRE	CCUUUAUUCUAAACAAACUGCCUA	Yes
mycl1b MRE	ACUUUAUGCUGUUUUCACUGCCUA	Yes
hells MRE	UGAUCAGUUUUGGCAAAGUCCACUGCCUG	No
rarab MRE	CAGUCAACAACAACACUGCCU	Yes
taxbp3 MRE	UAAUUAAUUAACACUAUUGCCU	No
Ikbkg MRE	AAAAAAGCUCAUCUGUACUGCCUU	Yes
tdrd7 MRE	UGAACAUCUACCCUUACUGUCU	No
gab1 MRE	AGAUCAGCUAGUUUACACUGCUUC	No
thbs4b MRE	CAAAUAUCAGCUAUAACUGCCUA	Yes
ptprg MRE	UAUGAAAAUAUCAGUGUUACUGCCUA	Yes
mta3 MRE	CCAUUUCCAAUAAAGACUGCCUG	No
hoxb8a MRE	UUCCAACAACAUGAAACUGCCUA	Yes
hoxa9a MRE	UAGUCACUUCACUGCCUU	No
creb1 MRE	CAGUCGCUGAUGGCUCUGCCUG	No
gadd45ba MRE	ACAUGAGCUGUGAAAGCUGCCUG	Yes
cmyb MRE1	UAACUUUUUGUUAUUCGCUGCCUU	No
cmyb MRE2	CAUACGUUUUUUAUACAAACUGCCUU	No
ttc25 MRE	GUCUUUAGUUAAGGUUUACUUUAUGACUGCCUU	Yes
mpp7 MRE	UAUUUUUUUUUAUAUAUCGGCUGCCUG	No
jag2a MRE	UCAUCUGUUCUCCUUCCGCGCCUGCCUU	No
mycb UTR	NM200172.1 1364-1645	No
creb1a UTR	NM200909.1 1075-1897	No
cmyb UTR	BC059803 1978-3131	No
ptprg UTR	Based on EST assembly	No
foxj1a UTR	NM001076706.2 1625-3442	No
foxj1b UTR	NM001008648.1 1549-2212	No
ttc25 UTR	NM200316.1 1561-1771	No
jag2a UTR	NM131862 3941-5269	No
hoxb8a UTR	NM131120.1 1116-1963	Yes
mpp7 UTR	NM130976.1 1786-4032	No
rfx2 UTR	NM001013278.1 2364-3607	No

Download Table S4

Download Table S5